RAD51AP1 compensates for the loss of RAD54 in homology-directed DNA repair

Platon Selemenakis[1,2], Neelam Sharma[1], Youngho Kwon[3], Mollie Uhrig[1], Patrick Sung[3] and Claudia Wiese[1]*

[1] Environmental and Radiological Health Sciences, Colorado State University, Fort Collins, Colorado, 80523, USA

[2] Cell and Molecular Biology Graduate Program, Colorado State University, Fort Collins, Colorado, 80523, USA

[3] Department of Biochemistry and Structural Biology, University of Texas Health San Antonio, San Antonio, Texas 78229, USA

* To whom correspondence should be addressed:

C.W. (email: Claudia.Wiese@colostate.edu)

Abstract

Homology-directed repair (HDR) is a complex DNA damage repair pathway and an attractive target of inhibition in anti-cancer therapy. To develop the most efficient inhibitors of HDR in cells, it is critical to identify compensatory sub-pathways.

In this study, we describe the synthetic interaction between RAD51AP1 and RAD54, two structurally unrelated proteins that function downstream of RAD51 in HDR. We show that deletion of both RAD51AP1 and RAD54 synergistically sensitizes human cancer cell lines to treatment with a Poly(adenosine 5´-diphosphate-ribose) polymerase inhibitor, to the DNA inter-strand crosslinking agent mitomycin C, and to hydroxyurea, which stalls the progression of DNA replication. We infer that HDR-directed anti-cancer treatment modalities shall consider this within-pathway functional overlap, and we hypothesize that in cancerous cells the simultaneous inactivation of both RAD54 and RAD51AP1 will accentuate tumor kill.

[*Keywords*: Homologous recombination, genome stability, synthetic lethality, RAD51AP1, RAD54, RAD54B]

Supplementary material is available.

Introduction

Homology-directed repair (HDR) is an essential DNA damage repair pathway critical for genome stability and tumor suppression. HDR is altered in many different tumor types and has become an attractive target for the development of new anti-cancer therapies (Kopa et al. 2019; Trenner and Sartori 2019). Accurate HDR is restricted to the S- and G2- phases of the cell cycle where the sister chromatid is used as the homologous template for the restoration of lost sequence information at the damaged DNA site. At the DNA break, a 3´-single-stranded (ss)DNA overhang is generated and protected by the ssDNA-binding protein RPA (Symington 2014; Daley et al. 2015). RPA is replaced by the RAD51 recombinase, a rate-limiting step in the HDR reaction that is dependent on the action of multiple recombination mediators (Sung 1997a; Sung 1997b; Dosanjh et al. 1998; Sung et al. 2003; Zhao et al. 2015; Belan et al. 2021; Roy et al. 2021). The RAD51-ssDNA nucleoprotein filament catalyzes the capture of the DNA template and initiates and the formation of a displacement loop (D-loop) with assistance of several RAD51-associated proteins (Petukhova et al. 1998; Tanaka et al. 2000; Miyagawa et al. 2002; Modesti et al. 2007; Wiese et al. 2007; Zhao et al. 2017).

RAD51AP1 and RAD54 are two RAD51-associated proteins that assist the RAD51 filament in the capture of the DNA donor molecule and in formation of the D-loop (Petukhova et al. 1998; Tanaka et al. 2000; Miyagawa et al. 2002; Modesti et al. 2007; Wiese et al. 2007; Zhao et al. 2017). RAD51AP1 may have evolved in response to the higher complexities of vertebrate genomes (Parplys et al. 2014). In contrast, RAD54 is highly conserved across eukaryotes (Clever et al. 1997; Essers et al. 1997; Golub et al. 1997; Petukhova et al. 1998; Swagemakers et al. 1998). RAD51AP1 functions in the protection of cells from genotoxic agents, in genome stability, and in the HDR-mediated alternative lengthening of telomeres (ALT) pathway (Henson et al. 2006; Modesti et al. 2007; Wiese et al. 2007; Barroso-Gonzalez et al. 2019). Similarly, RAD54 maintains HDR capability, cell survival after chemotherapeutic agents, and ALT activity (Swagemakers et al. 1998; Tan et al. 1999; Mason et al. 2015; Spies et al. 2016; Mason-Osann et al. 2020). Strikingly, in human cells, loss of either RAD51AP1 or RAD54 is associated with only a mild phenotype of HDR-deficiency (Henson et al. 2006; Modesti et al. 2007; Wiese et al. 2007; Gottipati et al. 2010; Spies et al. 2016; Olivieri et

al. 2020). Biochemically, both RAD51AP1 and RAD54 show similar effects on the stimulation of RAD51 activity in engaging the RAD51 filament with the homologous double-stranded (ds)DNA donor (*i.e*., synapsis) and in strand invasion (Petukhova et al. 1998; Petukhova et al. 1999; Solinger and Heyer 2001; Solinger et al. 2001; Sigurdsson et al. 2002; Modesti et al. 2007; Wiese et al. 2007). In these steps of the HDR reaction, RAD51AP1 may serve as an anchor between the two DNA molecules undergoing exchange (Modesti et al. 2007; Dunlop et al. 2012; Pires et al. 2021). In contrast, RAD54 belongs to the SWI2/SNF2 protein family of DNA-dependent ATPases (Flaus et al. 2006) and utilizes its ATPase activity to convert the synaptic complex into a D-loop (Sigurdsson et al. 2002; Crickard et al. 2020), to translocate along the DNA (Van Komen et al. 2000; Ristic et al. 2001) whereby chromatin is remodelled, and for the turnover of RAD51 (Alexiadis and Kadonaga 2002; Alexeev et al. 2003; Jaskelioff et al. 2003; Li and Heyer 2009).

The mild phenotype of RAD54-deficient human cells has been attributed to the existence of RAD54B, a RAD54 paralog (Hiramoto et al. 1999). Although less well understood than RAD54, evidence suggests that RAD54B also is involved in the core mechanisms of HDR (Tanaka et al. 2000; Miyagawa et al. 2002; Flaus et al. 2006; McManus et al. 2009; Ceballos and Heyer 2011). At the protein level, RAD54 and RAD54B share 48% identity and 63% similarity (Flaus et al. 2006; Ceballos and Heyer 2011), and when compared to RAD54 in biochemical studies, RAD54B was identified as the weaker ATPase (Tanaka et al. 2002). Although the exact roles of RAD54B in HDR in human cells remain to be determined, these results suggest that RAD54B may have less activity than RAD54 (Tanaka et al. 2002).

In this study, we show that in human cells loss of *RAD54* to a large extent can be compensated for by the RAD51AP1 protein, a structurally unrelated protein devoid of any DNA motor activity. We show that deletion of both *RAD54* and *RAD51AP1* synergistically sensitizes human cancer cell lines to treatment with the DNA inter-strand crosslinking agent mitomycin C (MMC), prolonged exposure to replication stalling by hydroxyurea (HU), and to Poly(adenosine 5´-diphosphate-ribose) polymerase inhibition (PARPi). We also show that the RAD54 paralog RAD54B can substitute for RAD54 activity, although, surprisingly, less universally than RAD51AP1. Based on these

results, we conclude that the activities of RAD51AP1 and RAD54 underpin two major routes for the completion of HDR downstream of RAD51 in human cells.

Results

Deletion of both RAD54 and RAD51AP1 synergistically sensitizes human cancer cell lines to the cytotoxic effects of MMC exposure

To investigate the genetic interaction between RAD51AP1 and RAD54, we generated double *RAD54*/*RAD51AP1* knockout (KO) HeLa cell lines and compared the phenotypes of these double KO cells to HeLa cells deleted for either *RAD51AP1* or *RAD54* that we have described earlier (Liang et al. 2019; Maranon et al. 2020). To generate *RAD54*/*RAD51AP1* double KO cells we targeted *RAD54* by CRISPR/Cas9-nic in *RAD51AP1* KO cells and selected two of several *RAD54*/*RAD51AP1* double KO clones for the experiments described below. In these cells, we verified loss of protein expression by Western blot analysis (Fig. 1A, lanes 5-6), sequenced across the Cas9-nic cleavage sites in *RAD54* to confirm mutagenesis (Supplemental Fig. S1A-C), and used immunocytochemistry to monitor loss of RAD54 foci formation after γ-irradiation (Supplemental Fig. S1D).

We determined the growth rates of all HeLa cell derivatives (*i.e.*, single KO and double KO cells) and detected no significant differences in population doubling times between single KO, double KO, and HeLa cells (Supplemental Fig. S1E). In fractionated protein extracts from unperturbed cells, we noted higher levels of RAD54 protein in *RAD51AP1* KO cells (Supplemental Fig. S1F, lanes 2 and 8) and higher levels of RAD51AP1 protein in *RAD54* KO cells (Supplemental Fig. S1F, lanes 9-10).

Next, we tested the sensitivity to MMC of single and double KO cells in clonogenic cell survival assays. In accord with our earlier studies (Liang et al. 2019; Maranon et al. 2020), we show that *RAD51AP1* and *RAD54* single KO cells are moderately sensitized to the cytotoxic effects of MMC exposure (Fig. 1B). Deletion of both *RAD51AP1* and *RAD54*, however, synergistically sensitized HeLa cells to MMC (Fig. 1B), suggesting a non-epistatic relation between RAD51AP1 and RAD54. To exclude that this effect was specific to HeLa cells, we depleted RAD51AP1 and/or RAD54 in A549 lung cancer cells

by siRNA (Supplemental Fig. S1G). A549 cells depleted for either RAD51AP1 or RAD54 showed similarly increased sensitivities to MMC while concomitant loss of both RAD51AP1 and RAD54 rendered A549 cells significantly more sensitive to the cytotoxic effects of MMC exposure (Fig. 1C). Collectively, these results reveal compensation between RAD51AP1 and RAD54 in the protection of human cells from MMC-induced DNA damage.

We used U2OS-DRGFP cells (Nakanishi et al. 2005; Xia et al. 2006) to assess the effects of RAD51AP1 and/or RAD54 depletion on gene conversion. Simultaneous depletion of both RAD51AP1 and RAD54 downregulated the levels of gene conversion at DRGFP ~ 10-fold ($p < 0.001$; Supplemental Fig. S1H), while single knockdown of either RAD51AP1 or RAD54 impaired gene conversion ~ 2-fold, as previously described (Wiese et al. 2007; Spies et al. 2016).

Next, we assessed the cell cycle progression upon MMC exposure of single and *RAD54*/*RAD51AP1* double KO cells by flow cytometry and compared the results to HeLa cells. In the absence of MMC, all cell lines progressed similarly through the cell cycle (Fig. 1D, left panel; Supplemental Fig. S1I). Twenty-four hours after release from MMC, all cell lines remained arrested in cell cycle progression and mainly in G2/M phase (Fig. 1D, middle panel; Supplemental Fig. S1I). At 72 h post release from MMC exposure, HeLa cells, *RAD51AP1* KO, and *RAD54* KO cells regained the capacity to proceed through mitosis and enter the following cell cycle. Both *RAD54/RAD51AP1* double KO cell lines, however, remained arrested in G2/M phase ($p < 0.0001$; Fig. 1D, right panel; Supplemental Fig. S1I), likely due to the higher fraction of unresolved or mis-repaired DNA damage remaining in these cells.

RAD54 deficiency is rescued by ectopic RAD54

Ectopic expression of HA-tagged RAD54 in *RAD54*/*RAD51AP1* double KO cells reverted their response to MMC to the level of *RAD51AP1* KO cells (Fig. 2A; Supplemental Fig. S2A). Similarly, cell cycle progression after MMC of *RAD54*/*RAD51AP1* double KO cells with ectopic RAD54 became similar to that of *RAD51AP1* KO cells (Fig. 2B; Supplemental Fig. S1I). Moreover, *RAD54*/*RAD51AP1*

double KO cells with ectopic RAD54 formed nuclear RAD54 foci after γ-irradiation (Supplemental Fig. S1D). Ectopic expression of RAD54 also rescued the sensitivity to MMC of single *RAD54* KO cells (Supplemental Fig. S2B,C) and RAD54 foci formation after γ-irradiation (Supplemental Fig. S1D). These results show that the phenotypes associated with *RAD54* deficiency in *RAD54*/*RAD51AP1* double KO and *RAD54* single KO cells stem from the loss of *RAD54*. However, ectopic expression of high amounts of RAD54 in *RAD51AP1* KO cells (Supplemental Fig. S2A, lanes 3-4) did not rescue the sensitivity of *RAD51AP1* KO cells to MMC (Fig. 2C), demonstrating that defined attributes of the RAD51AP1 protein cannot be compensated for by RAD54.

Deletion of both RAD51AP1 and RAD54 synergistically sensitizes HeLa cells to replication stress

We treated all cell lines with 4 mM HU for 5 hours, which blocks DNA synthesis and stalls replication fork movement (Liu et al. 2020). Extended fork stalling impairs fork recovery and replication restart (Bhat and Cortez 2018). To understand the fate of stalled forks in single and double KO cells, we monitored the recovery of cells from stalled replication using the single-molecule DNA fiber assay. To this end, we pulse-labeled cells with the thymidine analog 5-Chloro-2´-deoxyuridine (CldU) first, then replenished cells with HU-containing medium prior to pulse-labeling with 5-Iodo-2´-deoxyuridine (IdU) (Fig. 3A). We then determined the ability of all cell lines to restart replication by measuring the lengths of IdU tracts of CldU-labeled fibers (Fig. 3B). *RAD51AP1* KO cells showed no significant defect in fork restart compared to HeLa cells ($p = 0.0758$). In contrast, *RAD54* KO cells restarted forks significantly faster than HeLa cells ($p < 0.01$), possibly related to the role of RAD54 catalyzing fork regression (Bugreev et al. 2011). However, in comparison to both HeLa and single KO cells, *RAD54*/*RAD51AP1* double KO cells were significantly impaired in fork restart ($p < 0.0001$; Fig. 3C; Supplemental Fig. S3D; Table S2). Collectively, these results show that the efficient restart from stalled replication relies on RAD51AP1 or RAD54 in HeLa cells. The results suggest that RAD54 suppresses accelerated fork restart after HU, and that

RAD51AP1 helps overcome compromised fork stability from accelerated fork restart in *RAD54* KO cells.

In unperturbed cells, replication (as determined by IdU tract length of CldU-labeled fibers) progressed significantly slower in *RAD54*/*RAD51AP1* double KO cells than in HeLa or single KO cells, suggesting that endogenous obstacles to fork progression impede DNA replication in *RAD54*/*RAD51AP1* double KO cells (Fig. 3D).

In response to replication stress, replication forks reverse into four-way junctions through annealing of the nascent DNA strands (Zellweger et al. 2015). Fork reversal is mediated by RAD51 and many other HDR proteins, leading to the protection of replication forks from spurious nuclease attack (Thangavel et al. 2015; Zellweger et al. 2015; Mijic et al. 2017; Thakar and Moldovan 2021). To assess if RAD54 and/or RAD51AP1 function in the protection of replication forks from unprogrammed nuclease degradation, CldU tract lengths in cells exposed to HU were measured and compared to the CldU tract lengths in untreated cells (Supplementary Fig. S3A). CldU tracts after HU were shorter than those in unperturbed cells for all cell lines investigated (Supplementary Fig. S3B, C). Overall, however, CldU tracts in HU-treated *RAD51AP1* KO, *RAD54* KO, and *RAD54*/*RAD51AP1* double KO cells were not shorter than those in HU-treated HeLa cells (Table S1). These results suggest that RAD54 and RAD51AP1 largely function independently of the fork protection mechanism in overcoming replication stress in HeLa cells. We infer that replication forks in HeLa cells and the KO cell lines are degraded as part of the normal cellular physiology in response to prolonged fork stalling by HU (Thangavel et al. 2015), and that the recruitment of proteins involved in the protection of nascent DNA at replication forks likely is undisturbed in *RAD54*/*RAD51AP1* single and double KO cells.

Concomitant loss of RAD51AP1 and RAD54 exacerbates genome instability

Next, we tested the consequences of induced replication stress to cells with impaired replication restart. To this end, we determined chromatid gaps and breaks, and complex chromosome aberrations (*i.e.*, radials) in HeLa, single KO and *RAD54*/*RAD51AP1* double KO cells after treatment with HU (Fig. 3E, F). Exposure to HU led to 0.56±0.73

mean aberrations per metaphase in HeLa cells and to a significant increase in mean aberrations per metaphase in both *RAD51AP1* (0.91±1.02; $p < 0.01$) and *RAD54* single KO cells (1.03±1.07; $p < 0.0001$; Fig. 3G). As expected, in *RAD54*/*RAD51AP1* double KO cells, the mean number of aberrations per metaphase was further increased compared to single KO cells (1.53±1.30; $p < 0.0001$). Collectively, these results show that replication stress leads to genome instability most prominently in *RAD54*/*RAD51AP1* double KO cells, which also show the most pronounced defect in fork restart.

RAD54B compensates for RAD54 activity in the presence of RAD51AP1

The role of human RAD54B in HDR is not well understood. In mice, however, the contribution of Rad54B to HDR was discovered in the absence of Rad54 (Wesoly et al. 2006). To investigate the impact of RAD54B on the protection of human cells from MMC-induced DNA damage, we depleted RAD54B in HeLa, single KO, and *RAD54*/*RAD51AP1* double KO cells (Supplemental Fig. S4A) and performed MMC cell survival assays. Depletion of RAD54B in HeLa and *RAD51AP1* KO cells had no effect on their sensitivity to MMC (Fig. 4A). Similarly, depletion of RAD54B in *RAD54*/*RAD51AP1* double KO cells did not increase MMC cytotoxicity. In contrast, depletion of RAD54B in *RAD54* KO cells further sensitized *RAD54* KO cells to MMC ($p = 0.044$; Fig. 4A). These results show that, similar to what has been observed in mice (Wesoly et al. 2006), the activity of RAD54B is critical for the protection of human cells from MMC cytotoxicity in the absence of RAD54. In HeLa, *RAD51AP1* KO, and *RAD54*/*RAD51AP1* double KO cells, however, RAD54B appears to play no detectable role in the protection of cells from MMC-induced DNA damage.

To exclude the possibility that the mild increase in MMC sensitivity of *RAD54* KO cells depleted for RAD54B was the result of incomplete RAD54B knockdown, we generated *RAD54*/*RAD54B* double KO HeLa cells (Supplementary Fig. S4B-D) and compared their response to MMC to that of the *RAD54*/*RAD51AP1* double KOs. Similar to what we observed after RAD54B knockdown (Fig. 4A), two independently isolated *RAD54*/*RAD54B* double KO cells lines (KO-1 and KO-2) were significantly more

resistant to MMC than *RAD54*/*RAD51AP1* double KO cells ($p = 0.037$ and $p = 0.007$ for *RAD54*/*RAD54B* KO-1 and KO-2, respectively; Fig. 4B). These results show that in the absence of RAD54, human cells more heavily rely on RAD51AP1 than on RAD54B to resist MMC cytotoxicity.

To understand the consequences of concomitant RAD54 and RAD54B loss on replication fork dynamics, we used the DNA fiber assay, as described above, and measured the lengths of IdU tracts of CldU-labeled fibers in untreated cells and after HU (for schematic see Fig. 3A). As shown in Fig. 3D and herein determined independently, replication progresses significantly slower in *RAD54*/*RAD51AP1* double KO cells than in HeLa cells under unperturbed conditions ($p < 0.0001$; Fig. 4C; Table S1). In contrast, fork progression in unperturbed *RAD54*/*RAD54B* KO-1 and KO-2 cells was more similar to that of HeLa cells (Fig. 4C; Table S1). After HU, fork restart was significantly slower in *RAD54*/*RAD51AP1* double KO cells than in *RAD54*/*RAD54B* double KO cells ($p < 0.0001$; Fig. 4D; Table S1). These results show that, in response to stalled DNA replication in the absence of RAD54, the activities of both RAD51AP1 and RAD54B are important to efficiently restart replication forks. However, the absence of RAD51AP1 is more detrimental to the recovery from stalled replication than that of RAD54B.

RAD54B co-precipitates in anti-RAD51AP1 complexes

Since RAD54B knockdown did not further increase the sensitivity to MMC of *RAD51AP1* single and *RAD54/RAD51AP1* double KO cells, we hypothesized that this – in part – could be the result of RAD54B and RAD51AP1 acting in unity during the protection of cells from MMC-induced cytotoxicity. As such, we asked if RAD51AP1 may function in conjunction with RAD54B in human cells, and if a complex between these two proteins could be identified. Using the purified proteins, we previously showed that RAD51AP1 and RAD54 physically can interact, and that both proteins compete in binding to RAD51 (Maranon et al. 2020). Based on these results, we first tested if endogenous RAD54 would co-precipitate in anti-RAD51AP1 complexes of *RAD51AP1* KO cells stably expressing FLAG-tagged RAD51AP1. Our results show that RAD54 co-

precipitates with FLAG-RAD51AP1 under unperturbed conditions (Supplementary Fig. S4E, lane 4).

Next, we tested the association between RAD51AP1 and RAD54B in human cells. As RAD54B activity is more prevalent in the absence of RAD54 (Fig. 4A,B), we used *RAD54*/*RAD51AP1* double KO cells with transiently expressed eGFP-tagged RAD51AP1. Both RAD51 and RAD54B were present in anti-eGFP precipitates from *RAD54*/*RAD51AP1* double KO cells expressing eGFP-RAD51AP1 (Supplementary Fig. S4F, lane 7); in contrast, RAD54B was absent in anti-eGFP precipitates from *RAD54*/*RAD54B* double KO cells expressing eGFP-RAD51AP1 (Supplementary Fig. S4F, lane 8). We then prepared protein lysates from *RAD54*/*RAD51AP1* double KO cells transiently expressing eGFP-RAD51AP1 under unperturbed conditions (NT), and at 4 and 20 h after release from a 2-h treatment with 0.5 μM MMC. RAD54B was present in anti-eGFP complexes from both untreated and MMC exposed cells (Fig. 4E, lanes 6-7; Supplementary Fig. S4G, lanes 7-8). These results show that endogenous RAD54B can associate with ectopically expressed RAD51AP1 in *RAD54/RAD51AP1* double KO cells in the absence and in the presence of MMC-induced DNA damage.

Deletion of both RAD51AP1 and RAD54 synergistically sensitizes HeLa cells to olaparib

HDR deficiency selectively confers sensitivity to PARPi (Bryant et al. 2005; Farmer et al. 2005). Hence, we asked if single and *RAD54*/*RAD51AP1* double KO cells were sensitive to treatment with the PARPi olaparib. Compared to HeLa cells, *RAD51AP1* KO cells showed mildly increased sensitivity to olaparib ($p < 0.001$), while both *RAD54* KO cell lines (KO-1 and KO-2) were more sensitive than *RAD51AP1* KO cells ($p < 0.05$ and $p < 0.01$ for KO-1 and KO-2 compared to *RAD51AP1* KO cells, respectively; Fig. 5A). As observed after MMC, combined loss of both *RAD51AP1* and *RAD54* further sensitized cells to olaparib ($p < 0.05$ for *RAD51AP1*/*RAD54* KO-1 and KO-2 cells compared to the *RAD54* KO; Fig. 5A). Next, we compared the cytotoxicity to olaparib of *RAD54/RAD51AP1* double KO cells to that of the *RAD54/RAD54B* double KOs. Treatment with olaparib decreased the survival of both *RAD54*/*RAD51AP1* and

RAD54/*RAD54B* double KO cells to similar extend ($p < 0.0001$ compared to HeLa cells; Fig. 5B).

To understand why, in comparison to *RAD54*/*RAD54B* double KO cells, *RAD54*/*RAD51AP1* double KO cells respond with significantly increased sensitivity to MMC and HU albeit with similar sensitivity to olaparib, we analyzed the dynamics of replication fork progression by DNA fiber assay after a 1-day incubation of cells in 10 μM olaparib. Compared to untreated cells (Fig. 5C; Supplementary Fig. S5A), fiber tracts were longer in HeLa cells (Fig. 5D; Supplementary Fig. S5A; Table S1), consistent with the results from an earlier study (Maya-Mendoza et al. 2018). However, in *RAD54* single, and *RAD51AP1*/*RAD54* and *RAD54/RAD54B* double KO cells, fiber tracts were even longer than in HeLa cells ($p < 0.0001$; Fig. 5D; Supplementary Fig. S5A; Table S1), indicative of the further increased defects of the KO cell lines in restraining fork progression. Compared to the lengths of fiber tracts obtained under unperturbed conditions, median fiber tracts were 28% longer in HeLa cells, 33% longer in *RAD54* KO cells and 88% and 46% longer in *RAD54/RAD51AP1* and *RAD54/RAD54B* double KO cells, respectively. Collectively, these results show that HDR-proficient HeLa cells restrain accelerated fork elongation more effectively than *RAD54* single and *RAD54*/*RAD51AP1* and *RAD54*/*RAD54B* double KO cells. Moreover, while a 1-day exposure to olaparib is associated with increased levels of DSBs in all cell lines investigated, COMET assays revealed significantly more DSBs in *RAD54*/*RAD51AP1* and *RAD54*/*RAD54B* double KO cells than in HeLa cells and the *RAD54* single KO (Supplementary Fig. S5B,C; Table S2). These results suggest that fork stability is compromised when fork movement is accelerated, and that the stress to replication forks is higher in both *RAD51AP1*/*RAD54* and *RAD54*/*RAD54B* double KO cells than in the *RAD54* single KO.

Discussion

Our study uncovered extensive functional overlap between RAD51AP1 and RAD54 in human cancer cell lines. Based on these results, we suggest that a RAD54-independent HDR back-up pathway exists that most universally relies on the activity of RAD51AP1

(Fig. 6). Given that a complex between RAD51AP1 and RAD54B can be isolated (this study) and evidence of an indirect association between human RAD54B and RAD51 within the chromatin environment and in cells (Tanaka et al. 2000; Zhang et al. 2007), it is possible that in select stages of the HDR reaction, within a certain context of the genome, or in response to specific types of DNA damage, RAD51AP1 may function cooperatively with RAD54B, possibly bridging RAD54B to RAD51 or stabilizing the RAD54B-RAD51 association. Of note, an earlier study showed that RAD54B has less ATPase activity than RAD54 (Tanaka et al. 2002). Thus, in the absence of RAD54, RAD51AP1 may support RAD54B function during synapsis and strand invasion.

In response to MMC, *RAD54* KO cells with RAD54B knockdown showed significantly increased sensitivity while no increase in cytotoxicity was detected in *RAD54*/*RAD51AP1* double KO cells with RAD54B knockdown. These results could suggest that RAD54B may not be active in *RAD54*/*RAD51AP1* double KO cells, which - in addition to RAD54 - lack the expression of RAD51AP1. However, *RAD54*/*RAD51AP1* double KO cells are significantly more sensitive to MMC than *RAD54*/*RAD54B* double KO cells, which argues that RAD51AP1 can function independently of RAD54B upon treatment of cells with MMC (Fig. 6A). This could either be together with another and yet to be identified translocase, or within transcriptionally active, decondensed regions of the genome in which RAD51AP1 specifically was shown to promote HDR (Ouyang et al. 2021).

The RAD54 translocase is a DNA motor protein with many roles in HDR-mediated DSB repair (Ceballos and Heyer 2011). While mutants of the orthologous Rad54 protein in *S. cerevisiae* are highly sensitive to ionizing radiation (Game and Mortimer 1974; Calderon et al. 1983), loss of RAD54 function in human cells and mice is associated with a comparatively mild phenotype (Essers et al. 1997; Swagemakers et al. 1998; Gottipati et al. 2010; Spies et al. 2016), suggesting that other proteins may compensate for RAD54 activity in mammalian cells. That RAD54B could be one such protein was suspected from the experiments carried out in mice (Wesoly et al. 2006; Kirshner et al. 2009). Yet, a study directly testing the synthetic interaction between human RAD54 and RAD54B had not been available. Our study helped to address this knowledge gap. We show that, in the absence of RAD54, RAD54B function becomes important for the

protection of human cells from MMC cytotoxicity, HU-induced replication stress and, particularly, for cellular resistance to olaparib, a drug that leads to accelerated replication fork progression (Maya-Mendoza et al. 2018; Thakar and Moldovan 2021). However, in the context of MMC and HU, agents that more immediately lead to stalled and collapsed DNA replication (Rickman et al. 2020; Thakar and Moldovan 2021), the presence of RAD51AP1, surprisingly, is more than equally important than the presence of RAD54B. As such, our results also help explain the comparatively mild phenotypes of human cells with RAD51AP1 deficiency (Henson et al. 2006; Modesti et al. 2007; Wiese et al. 2007), as most of the RAD51AP1 activity apparently can be compensated for by RAD54.

Fork protection confers PARPi-resistance (Ray Chaudhuri et al. 2016; Cantor and Calvo 2017), and both *RAD54*/*RAD51AP1* and *RAD54*/*RAD54B* double KO cells are exquisitely sensitive to olaparib. Yet, based on our results, RAD54, RAD51AP1, and RAD54B appear to play no major role in the fork protection pathway (Supplementary Fig. S3C). In contrast, upon treatment of cells with HU, longer CldU tracts are detected in all KO cell lines compared to HeLa cells, potentially related to suppressed fork reversal in the absence of RAD54 (Bugreev et al. 2011).

PARPi treatment leads to the formation of replication associated ssDNA gaps (Maya-Mendoza et al. 2018; Thakar and Moldovan 2021), and HDR-mediated post-replicative repair to eliminate these ssDNA replication gaps (Hashimoto et al. 2010; Piberger et al. 2020). We speculate that concomitant loss of RAD54 and either RAD51AP1 or RAD54B may exacerbate ssDNA gap formation, leading to the increased sensitivity to olaparib of double KO cells compared to the *RAD54* single KO (Fig. 6B).

Taken together, we show that RAD54 function can be largely compensated for by the RAD51AP1 protein. Surprisingly, in the context of stalled and collapsed DNA replication (after HU and MMC), the compensatory activity of RAD51AP1 is greater than that of RAD54B. After treatment of cells with olaparib, however, RAD51AP1 and RAD54B are equally important in substituting for RAD54, which may stem from the similar degree of engagement of both proteins in post-replication repair.

RAD51AP1 expression is increased in different breast cancer subtypes and other cancers and inversely associated with overall survival (Song et al. 2004; Henson et al. 2006; Martin et al. 2007; Martinez et al. 2007; Obama et al. 2008; Pathania et al. 2016; Chudasama et al. 2018; Li et al. 2018; Bridges et al. 2020; Zhao et al. 2020; Zhuang et al. 2020). Moreover, *Rad51ap1* deficiency in mice abrogates tumor growth and metastasis in a breast cancer model (Bridges et al. 2020), suggesting that the RAD51AP1 protein may be a promising target of inhibition in anti-cancer therapy. Given our results, that show extensive redundancy between RAD51AP1 and RAD54, we predict that the simultaneous inactivation of both RAD51AP1 and RAD54 will more significantly sensitize cancer cells to chemotherapy and thereby could lead to the much-wanted reduction in dose with the consequence of diminished side effects. Targeting both RAD51AP1 and RAD54 may be particularly effective against tumors with overactive HDR (Raderschall et al. 2002; Xu et al. 2005; Klein 2008; Marsden et al. 2016), cancerous cells which maintain their telomeres by the ALT pathway (Barroso-Gonzalez et al. 2019; Mason-Osann et al. 2020; Recagni et al. 2020), and BRCA1/2-mutant tumors that have regained HDR proficiency and developed resistance to PARPi (Han et al. 2020; Kim et al. 2021).

Materials and methods

Cell culture, transfections, and siRNAs

HeLa and A549 cells were obtained from ATCC and were maintained as recommended. HeLa cells in which *RAD51AP1* or *RAD54* were deleted by CRISPR/Cas9n(D10A) were maintained as described earlier (Liang et al. 2019; Maranon et al. 2020). Small interfering RNAs (siRNAs) were obtained from Qiagen (Valencia, CA). For the non-depleting negative control siRNA, the following target sequence was used: 5´-GATTCGAACGTGTCACGTCAA-3´ (Zafar et al. 2010; Parplys et al. 2015). The target siRNA sequences to knockdown RAD54, RAD54B and RAD51AP1 were 5´-AAGCATTTATTCGAAGCATTT-3´, 5´-ACCCAAGAAATTATAAATAAA-3´ and 5´-AACCTCATATCTCTAATTGCA-3´ (Modesti et al. 2007; Wiese et al. 2007; Zafar et al. 2010; Parplys et al. 2015), respectively. SiRNA forward transfections were performed

using lipofectamine RNAiMAX (Invitrogen, Carlsbad, CA) on two consecutive days and according to the instructions of the manufacturer (Invitrogen, Carlsbad, CA). The concentration of siRNAs in transfections was 20 nM each. Cells were treated with drugs at 96 h after the first transfection, and the extent of protein knockdown or expression was assessed by Western blot analysis.

Generation of RAD51AP1/RAD54 double KO cells

RAD51AP1 knockout (KO) cells were used to generate *RAD51AP1*/*RAD54* double KO (R54/AP1 DKO) cells as described for the generation of *RAD54* KO cells (Maranon et al. 2020). Briefly, a combination of two *RAD54* CRISPR/Cas9n(D10A) KO plasmids each containing one of two different sgRNAs (*i.e.*, sgRNA (54)-A and sgRNA (54)-B; Table S3) was purchased from Santa Cruz Biotechnology (sc-401750-NIC) and used to transfect *RAD51AP1* KO cells with Lipofectamine2000 (Invitrogen). Twenty-four hours post transfection, cells were selected for two days in 2 µg/ml puromycin and then trypsinized and reseeded at 0.5 cells/well in 96-well pates. Single clones were picked after two weeks and expanded in normal growth medium. Successful elimination of RAD54 protein was confirmed by Western blot analysis and by immunocytochemistry (ICC) after exposure of cells to 8 Gy of γ-rays. In addition, *RAD54* disruption was validated by sequence analysis after genomic DNA was isolated from a selection of edited and non-edited clonal isolates using DNeasy Blood & Tissue Kit (Qiagen). The *RAD54* genomic sequence containing the two sgRNA target sequences was amplified by PCR using primers flanking the sgRNA target sites (Table S3). PCR products were gel purified and cloned into pCR4-TOPO (Invitrogen, Carlsbad, CA), transformed into TOP10 competent *E. coli*, plasmid DNA was prepared using ZR Plasmid Miniprep-Classic Kit (Zymo Research, Irvine, CA) and submitted for Sanger sequencing.

Generation of RAD54 expressing RAD51AP1 KO, RAD54 KO and RAD54/RAD51AP1 DKO cells

The plasmid containing the C-terminally HA-tagged full-length human RAD54 cDNA has been described elsewhere (Maranon et al. 2020). A *Kpn*I to *Not*I digest was performed to clone RAD54-HA into pENTR1A (Invitrogen), followed by transfer into pLentiCMV/TO DEST#2 (Campeau et al. 2009) using Gateway LR Clonase II (Invitrogen) for the production of lentiviral particles in HEK293FT cells (Invitrogen), as described (Campeau et al. 2009). Lentivirus was used to transduce *RAD51AP1* KO, *RAD54* KO, and *RAD54*/*RAD51AP1* double KO cells in 6 µg/ml polybrene, as described (Campeau et al. 2009). Forty-eight hours after transduction, cells were trypsinized and seeded in 96-well cell culture plates at a density of 0.5 cells/well in the presence of 0.75 µg/ml puromycin for the selection of clonal isolates. Stable expression of RAD54 protein in isolated clones was confirmed by Western blot analysis and ICC.

Cell fractionation and cell growth assay

Cell fractionation was carried out using the Subcellular Protein Fractionation Kit (Thermo Fisher Scientific, Waltham, MA) and as described by the manufacturer. To determine the rates of cell growth, cells were seeded in 6-well tissue culture plates at a density of 1.2×10^4 cells/well. Cell were counted after trypsinization for eight consecutive days. Cell numbers were plotted using nonlinear regression, and population doubling times (PDL) were calculated using the following equation:

$$\mathrm{PDL} = 3.32 \times \log\left(\frac{\text{total viable cells at harvest}}{\text{total viable cells at seed}}\right)$$

Clonogenic cell survival assays and Western blot analysis

Clonogenic cell survival assays after mitomycin C (MMC; Sigma, St. Louis, MO) were performed as described (Maranon et al. 2020). To assess cellular sensitivity to olaparib (AZD2281; KU-0059436; Selleck Chemicals, Houston, TX), cells were chronically exposed to 0.5-2.5 µM olaparib in regular growth medium for 12 days, as described (Spies et al. 2016). Following the incubation, cells were fixed and stained with crystal violet to visualize colonies and determine the fraction of cells surviving.

Western blot analyses were performed according to our standard protocols (Wiese et al. 2006; Parplys et al. 2014; Zhao et al. 2015; Maranon et al. 2020). To detect proteins of interest the following primary antibodies were used: α-RAD51AP1 ((Dray et al. 2010); 1:6,000), α-RAD54 (F-11; sc-374598; Santa Cruz Biotechnology; 1:1,000); α-RAD51 (Ab-1; EMD Millipore; 1:3,000), α-PARP1 (ab6079; Abcam; 1:2,000), α-β-Actin (ab8226;Abcam; 1:1,000) and α-RAD54B ((Wesoly et al. 2006); 1:1,000). HRP-conjugated goat anti-rabbit or goat anti-mouse IgG (Jackson ImmunoResearch Laboratories, West Grove, PA; 1:10,000) were used as secondary antibodies. Western blot signals were acquired using a Chemidoc XRS+ gel imaging system and Image Lab software version 5.2.1 (BioRad).

Cell cycle analysis and flow cytometry

Cell cycle analysis and flow cytometry were performed essentially as described earlier (Maranon et al. 2020), except that exponentially growing cells were treated with 0.5 μM MMC for 2 hours, washed twice with warm PBS and incubated in fresh growth medium for the times indicated prior to pulse-labeling with 10 μM EdU.

Indirect immunostaining, microscopy, and image analysis

Indirect immunostaining was performed as described (Maranon et al. 2020). The primary antibody used to detect RAD54 foci was α-RAD54 (F-11; sc-374598; Santa Cruz Biotechnology; 1:1,000). A Zeiss Axio-Imager.Z2 microscope equipped with Zen Blue software (Carl Zeiss Microscopy) was used to take images using a 63x oil objective. In each channel, 18 Z-stacks were obtained as 0.2 μm slices. Images were processed in Fiji (https://imagej.net/Fiji), separating the channels and producing maximum projection files.

Metaphase spreads

For the assessment of chromosomal aberrations, $2x10^5$ cells were seeded in 6-well tissue culture plates and incubated at 37°C for 24 hours before exposure to 4 mM hydroxyurea (HU; Sigma) in regular growth medium for 5 hours, as described (Schlacher et al. 2011). After HU treatment, cells were washed in warm PBS and incubated in medium containing 0.1 µg/ml colcemid (SERVA) for 24 hours. To produce metaphase spreads, cells were detached and allowed to swell in 0.075 M KCl at 37°C for 30 minutes and fixed in methanol:acetic acid (3:1), as described (Parplys et al. 2015). Cells were dropped on slightly tilted wet slides, air dried and stained in 3% Giemsa in Sorensen buffer (0.2 M Na_2HPO_4/NaH_2PO4, pH7.3) at room temperature for 10 min. Images were acquired using Zeiss Axio-Imager.Z2 microscope equipped with Zen Blue software (Carl Zeiss Microscopy) using a 63x oil objective. One hundred metaphases were assessed per sample.

DNA fiber assay

DNA replication progression was assessed by the single-molecule DNA fiber assay and essentially as described previously (Schlacher et al. 2011; Parplys et al. 2015; Taglialatela et al. 2017). Briefly, exponentially growing cells were pulse-labelled in regular growth medium containing 25 µM CldU for 20 min, followed by a 5-h incubation in regular growth medium with 4 mM HU, after which the cells were pulse-labelled in regular growth medium containing 250 µM IdU for 20 min. In a modified version of this assay, cells were exposed for 24 h in 10 µM olaparib, prior to two consecutive rounds of 20 min each with CldU first and then with IdU (Maya-Mendoza et al. 2018). Per sample and condition, 200 fibers were scored, and data were plotted in Prism 8 GraphPad.

Co-immunoprecipitations

The peGFP-RAD51AP1 expression vector is based on peGFP-C1 (Clontech) and has been described previously (Modesti et al. 2007). *RAD54*/*RAD51AP1* double KO cells were transfected with peGFP-C1 or peGFP-RAD51AP1 and Lipofectamine2000 (Invitrogen), as specified by the manufacturer. Twenty-four hours after transfection, cells

were subjected to a medium change or treated with 0.5 μM MMC for 2 hours. Following MMC treatment, cells were washed twice with warm PBS, fresh medium was added, and cells were incubated for the times indicated. Cells were lysed in chilled lysis buffer containing 50 mM Tris-HCl, pH 7.5, 300 mM NaCl, and 0.5% NP-40, supplemented with EDTA-free protease inhibitor cocktail (Roche) and HALT phosphatase inhibitors (ThermoScientific). For $1.5x10^6$ cells, 25 μl of GFP-Trap ® dynabeads (ChromoTek) were used to trap the ectopic proteins. Protein lysates were diluted to 50 mM Tris-HCl, pH 7.5, 150 mM NaCl, 0.1% NP-40, and 0.1unit DNase I (Gold Biotechnology) per μg protein, and mixed with the equilibrated beads at 4°C for 1 h with gentle rotation. The GFP-Trap ® dynabeads were washed 3× with 500 μl binding buffer, bound protein complexes were eluted in 40 μl 2× LDS buffer (Thermo Fisher Scientific) and fractionated on 7% NuPAGE Tris-Acetate gels (Thermo Fisher Scientific) and for Western blot analysis.

Statistics and reproducibility

Prism 8 GraphPad Software was used to perform statistical analysis. Data obtained are from 2-4 independent experiments, as indicated. To assess statistical significance two-way or one-way ANOVA tests were performed. $P \leq 0.05$ was considered significant.

Data availability

All data supporting the findings of this study are available here and in the Supplemental Material.

Competing interest statement

The authors declare no competing interests.

Acknowledgements

The authors wish to thank the CSU Flow Cytometry and Cell Sorting Facility for their help in method optimization and sample analyses. This work was supported by a CSU CVMBS College Research Grant and by National Institutes of Health Grants R01ES021454, R56ES021454, R03ES029206 (to C.W.) and R01ES007061, R35CA241801 (to P.S.).

Author contributions: Y.K., P.S. and C.W. conceptualization; P.S., N.S., Y.K. and M.U. data curation; P.S., N.S., Y.K. and M.U. data analyses and validation; P.S., N.S., Y.K., P.S. and C.W. writing of the manuscript; P.S. and C.W. funding acquisition.

References

Alexeev A, Mazin A, Kowalczykowski SC. 2003. Rad54 protein possesses chromatin-remodeling activity stimulated by the Rad51-ssDNA nucleoprotein filament. *Nat Struct Biol* **10**: 182-186.

Alexiadis V, Kadonaga JT. 2002. Strand pairing by Rad54 and Rad51 is enhanced by chromatin. *Genes & development* **16**: 2767-2771.

Barroso-Gonzalez J, Garcia-Exposito L, Hoang SM, Lynskey ML, Roncaioli JL, Ghosh A, Wallace CT, Modesti M, Bernstein KA, Sarkar SN et al. 2019. RAD51AP1 Is an Essential Mediator of Alternative Lengthening of Telomeres. *Molecular cell* **76**: 217.

Belan O, Barroso C, Kaczmarczyk A, Anand R, Federico S, O'Reilly N, Newton MD, Maeots E, Enchev RI, Martinez-Perez E et al. 2021. Single-molecule analysis reveals cooperative stimulation of Rad51 filament nucleation and growth by mediator proteins. *Molecular cell* **81**: 1058-1073 e1057.

Bhat KP, Cortez D. 2018. RPA and RAD51: fork reversal, fork protection, and genome stability. *Nat Struct Mol Biol* **25**: 446-453.

Bridges AE, Ramachandran S, Pathania R, Parwal U, Lester A, Rajpurohit P, Morera DS, Patel N, Singh N, Korkaya H et al. 2020. RAD51AP1 Deficiency Reduces Tumor Growth by Targeting Stem Cell Self-Renewal. *Cancer Res* **80**: 3855-3866.

Bryant HE, Schultz N, Thomas HD, Parker KM, Flower D, Lopez E, Kyle S, Meuth M, Curtin NJ, Helleday T. 2005. Specific killing of BRCA2-deficient tumours with inhibitors of poly(ADP-ribose) polymerase. *Nature* **434**: 913-917.

Bugreev DV, Rossi MJ, Mazin AV. 2011. Cooperation of RAD51 and RAD54 in regression of a model replication fork. *Nucleic Acids Res* **39**: 2153-2164.

Calderon IL, Contopoulou CR, Mortimer RK. 1983. Isolation and characterization of yeast DNA repair genes : II. Isolation of plasmids that complement the mutations rad50-1, rad51-1, rad54-3, and rad55-3. *Curr Genet* **7**: 93-100.

Campeau E, Ruhl VE, Rodier F, Smith CL, Rahmberg BL, Fuss JO, Campisi J, Yaswen P, Cooper PK, Kaufman PD. 2009. A versatile viral system for expression and depletion of proteins in mammalian cells. *PLoS One* **4**: e6529.

Cantor SB, Calvo JA. 2017. Fork Protection and Therapy Resistance in Hereditary Breast Cancer. *Cold Spring Harb Symp Quant Biol* **82**: 339-348.

Ceballos SJ, Heyer WD. 2011. Functions of the Snf2/Swi2 family Rad54 motor protein in homologous recombination. *Biochim Biophys Acta* **1809**: 509-523.

Chudasama D, Bo V, Hall M, Anikin V, Jeyaneethi J, Gregory J, Pados G, Tucker A, Harvey A, Pink R et al. 2018. Identification of cancer biomarkers of prognostic value using specific gene regulatory networks (GRN): a novel role of RAD51AP1 for ovarian and lung cancers. *Carcinogenesis* **39**: 407-417.

Clever B, Interthal H, Schmuckli-Maurer J, King J, Sigrist M, Heyer WD. 1997. Recombinational repair in yeast: functional interactions between Rad51 and Rad54 proteins. *EMBO J* **16**: 2535-2544.

Crickard JB, Moevus CJ, Kwon Y, Sung P, Greene EC. 2020. Rad54 Drives ATP Hydrolysis-Dependent DNA Sequence Alignment during Homologous Recombination. *Cell* **181**: 1380-1394 e1318.

Daley JM, Niu H, Miller AS, Sung P. 2015. Biochemical mechanism of DSB end resection and its regulation. *DNA repair* **32**: 66-74.

Dosanjh MK, Collins DW, Fan W, Lennon GG, Albala JS, Shen Z, Schild D. 1998. Isolation and characterization of RAD51C, a new human member of the RAD51 family of related genes. *Nucleic Acids Res* **26**: 1179-1184.

Dray E, Etchin J, Wiese C, Saro D, Williams GJ, Hammel M, Yu X, Galkin VE, Liu D, Tsai MS et al. 2010. Enhancement of RAD51 recombinase activity by the tumor suppressor PALB2. *Nat Struct Mol Biol* **17**: 1255-1259.

Dunlop MH, Dray E, Zhao W, San Filippo J, Tsai MS, Leung SG, Schild D, Wiese C, Sung P. 2012. Mechanistic insights into RAD51-associated protein 1 (RAD51AP1) action in homologous DNA repair. *The Journal of biological chemistry* **287**: 12343-12347.

Essers J, Hendriks RW, Swagemakers SM, Troelstra C, de Wit J, Bootsma D, Hoeijmakers JH, Kanaar R. 1997. Disruption of mouse RAD54 reduces ionizing radiation resistance and homologous recombination. *Cell* **89**: 195-204.

Farmer H, McCabe N, Lord CJ, Tutt AN, Johnson DA, Richardson TB, Santarosa M, Dillon KJ, Hickson I, Knights C et al. 2005. Targeting the DNA repair defect in BRCA mutant cells as a therapeutic strategy. *Nature* **434**: 917-921.

Flaus A, Martin DM, Barton GJ, Owen-Hughes T. 2006. Identification of multiple distinct Snf2 subfamilies with conserved structural motifs. *Nucleic Acids Res* **34**: 2887-2905.

Game JC, Mortimer RK. 1974. A genetic study of x-ray sensitive mutants in yeast. *Mutation research* **24**: 281-292.

Golub EI, Kovalenko OV, Gupta RC, Ward DC, Radding CM. 1997. Interaction of human recombination proteins Rad51 and Rad54. *Nucleic Acids Res* **25**: 4106-4110.

Gottipati P, Vischioni B, Schultz N, Solomons J, Bryant HE, Djureinovic T, Issaeva N, Sleeth K, Sharma RA, Helleday T. 2010. Poly(ADP-ribose) polymerase is hyperactivated in homologous recombination-defective cells. *Cancer Res* **70**: 5389-5398.

Han Y, Yu X, Li S, Tian Y, Liu C. 2020. New Perspectives for Resistance to PARP Inhibitors in Triple-Negative Breast Cancer. *Front Oncol* **10**: 578095.

Hashimoto Y, Ray Chaudhuri A, Lopes M, Costanzo V. 2010. Rad51 protects nascent DNA from Mre11-dependent degradation and promotes continuous DNA synthesis. *Nat Struct Mol Biol* **17**: 1305-1311.

Henson SE, Tsai SC, Malone CS, Soghomonian SV, Ouyang Y, Wall R, Marahrens Y, Teitell MA. 2006. Pir51, a Rad51-interacting protein with high expression in aggressive lymphoma, controls mitomycin C sensitivity and prevents chromosomal breaks. *Mutation research* **601**: 113-124.

Hiramoto T, Nakanishi T, Sumiyoshi T, Fukuda T, Matsuura S, Tauchi H, Komatsu K, Shibasaki Y, Inui H, Watatani M et al. 1999. Mutations of a novel human RAD54 homologue, RAD54B, in primary cancer. *Oncogene* **18**: 3422-3426.

Jaskelioff M, Van Komen S, Krebs JE, Sung P, Peterson CL. 2003. Rad54p is a chromatin remodeling enzyme required for heteroduplex DNA joint formation with chromatin. *J Biol Chem* **278**: 9212-9218.

Kim DS, Camacho CV, Kraus WL. 2021. Alternate therapeutic pathways for PARP inhibitors and potential mechanisms of resistance. *Exp Mol Med*.

Kirshner M, Rathavs M, Nizan A, Essers J, Kanaar R, Shiloh Y, Barzilai A. 2009. Analysis of the relationships between ATM and the Rad54 paralogs involved in homologous recombination repair. *DNA repair* **8**: 253-261.

Klein HL. 2008. The consequences of Rad51 overexpression for normal and tumor cells. *DNA repair* **7**: 686-693.

Kopa P, Macieja A, Galita G, Witczak ZJ, Poplawski T. 2019. DNA Double Strand Breaks Repair Inhibitors: Relevance as Potential New Anticancer Therapeutics. *Curr Med Chem* **26**: 1483-1493.

Kovalenko OV, Golub EI, Bray-Ward P, Ward DC, Radding CM. 1997. A novel nucleic acid-binding protein that interacts with human rad51 recombinase. *Nucleic Acids Res* **25**: 4946-4953.

Li S, Xuan Y, Gao B, Sun X, Miao S, Lu T, Wang Y, Jiao W. 2018. Identification of an eight-gene prognostic signature for lung adenocarcinoma. *Cancer Manag Res* **10**: 3383-3392.

Li X, Heyer WD. 2009. RAD54 controls access to the invading 3'-OH end after RAD51-mediated DNA strand invasion in homologous recombination in Saccharomyces cerevisiae. *Nucleic Acids Res* **37**: 638-646.

Liang F, Miller AS, Longerich S, Tang C, Maranon D, Williamson EA, Hromas R, Wiese C, Kupfer GM, Sung P. 2019. DNA requirement in FANCD2 deubiquitination by

USP1-UAF1-RAD51AP1 in the Fanconi anemia DNA damage response. *Nat Commun* **10**: 2849.

Liu W, Krishnamoorthy A, Zhao R, Cortez D. 2020. Two replication fork remodeling pathways generate nuclease substrates for distinct fork protection factors. *Sci Adv* **6**.

Maranon DG, Sharma N, Huang Y, Selemenakis P, Wang M, Altina N, Zhao W, Wiese C. 2020. NUCKS1 promotes RAD54 activity in homologous recombination DNA repair. *J Cell Biol* **219**.

Marsden CG, Jensen RB, Zagelbaum J, Rothenberg E, Morrical SW, Wallace SS, Sweasy JB. 2016. The Tumor-Associated Variant RAD51 G151D Induces a Hyper-Recombination Phenotype. *PLoS Genet* **12**: e1006208.

Martin RW, Orelli BJ, Yamazoe M, Minn AJ, Takeda S, Bishop DK. 2007. RAD51 up-regulation bypasses BRCA1 function and is a common feature of BRCA1-deficient breast tumors. *Cancer Res* **67**: 9658-9665.

Martinez I, Wang J, Hobson KF, Ferris RL, Khan SA. 2007. Identification of differentially expressed genes in HPV-positive and HPV-negative oropharyngeal squamous cell carcinomas. *Eur J Cancer* **43**: 415-432.

Mason JM, Dusad K, Wright WD, Grubb J, Budke B, Heyer WD, Connell PP, Weichselbaum RR, Bishop DK. 2015. RAD54 family translocases counter genotoxic effects of RAD51 in human tumor cells. *Nucleic Acids Res* **43**: 3180-3196.

Mason-Osann E, Terranova K, Lupo N, Lock YJ, Carson LM, Flynn RL. 2020. RAD54 promotes alternative lengthening of telomeres by mediating branch migration. *EMBO Rep* **21**: e49495.

Maya-Mendoza A, Moudry P, Merchut-Maya JM, Lee M, Strauss R, Bartek J. 2018. High speed of fork progression induces DNA replication stress and genomic instability. *Nature* **559**: 279-284.

McManus KJ, Barrett IJ, Nouhi Y, Hieter P. 2009. Specific synthetic lethal killing of RAD54B-deficient human colorectal cancer cells by FEN1 silencing. *Proc Natl Acad Sci U S A* **106**: 3276-3281.

Mijic S, Zellweger R, Chappidi N, Berti M, Jacobs K, Mutreja K, Ursich S, Ray Chaudhuri A, Nussenzweig A, Janscak P et al. 2017. Replication fork reversal triggers fork degradation in BRCA2-defective cells. *Nat Commun* **8**: 859.

Miyagawa K, Tsuruga T, Kinomura A, Usui K, Katsura M, Tashiro S, Mishima H, Tanaka K. 2002. A role for RAD54B in homologous recombination in human cells. *EMBO J* **21**: 175-180.

Modesti M, Budzowska M, Baldeyron C, Demmers JA, Ghirlando R, Kanaar R. 2007. RAD51AP1 is a structure-specific DNA binding protein that stimulates joint molecule formation during RAD51-mediated homologous recombination. *Molecular cell* **28**: 468-481.

Nakanishi K, Yang YG, Pierce AJ, Taniguchi T, Digweed M, D'Andrea AD, Wang ZQ, Jasin M. 2005. Human Fanconi anemia monoubiquitination pathway promotes homologous DNA repair. *Proc Natl Acad Sci U S A* **102**: 1110-1115.

Obama K, Satoh S, Hamamoto R, Sakai Y, Nakamura Y, Furukawa Y. 2008. Enhanced expression of RAD51 associating protein-1 is involved in the growth of intrahepatic cholangiocarcinoma cells. *Clin Cancer Res* **14**: 1333-1339.

Olivieri M, Cho T, Alvarez-Quilon A, Li K, Schellenberg MJ, Zimmermann M, Hustedt N, Rossi SE, Adam S, Melo H et al. 2020. A Genetic Map of the Response to DNA Damage in Human Cells. *Cell* **182**: 481-496 e421.

Ouyang J, Yadav T, Zhang JM, Yang H, Rheinbay E, Guo H, Haber DA, Lan L, Zou L. 2021. RNA transcripts stimulate homologous recombination by forming DR-loops. *Nature* **594**: 283-288.

Parplys AC, Kratz K, Speed MC, Leung SG, Schild D, Wiese C. 2014. RAD51AP1-deficiency in vertebrate cells impairs DNA replication. *DNA repair* **24**: 87-97.

Parplys AC, Zhao W, Sharma N, Groesser T, Liang F, Maranon DG, Leung SG, Grundt K, Dray E, Idate R et al. 2015. NUCKS1 is a novel RAD51AP1 paralog important for homologous recombination and genome stability. *Nucleic Acids Res* **43**: 9817-9834.

Pathania R, Ramachandran S, Mariappan G, Thakur P, Shi H, Choi JH, Manicassamy S, Kolhe R, Prasad PD, Sharma S et al. 2016. Combined Inhibition of DNMT and

HDAC Blocks the Tumorigenicity of Cancer Stem-like Cells and Attenuates Mammary Tumor Growth. *Cancer Res* **76**: 3224-3235.

Petukhova G, Stratton S, Sung P. 1998. Catalysis of homologous DNA pairing by yeast Rad51 and Rad54 proteins. *Nature* **393**: 91-94.

Petukhova G, Van Komen S, Vergano S, Klein H, Sung P. 1999. Yeast Rad54 promotes Rad51-dependent homologous DNA pairing via ATP hydrolysis-driven change in DNA double helix conformation. *J Biol Chem* **274**: 29453-29462.

Piberger AL, Bowry A, Kelly RDW, Walker AK, Gonzalez-Acosta D, Bailey LJ, Doherty AJ, Mendez J, Morris JR, Bryant HE et al. 2020. PrimPol-dependent single-stranded gap formation mediates homologous recombination at bulky DNA adducts. *Nat Commun* **11**: 5863.

Pires E, Sharma N, Selemenakis P, Wu B, Huang Y, Alimbetov DS, Zhao W, Wiese C. 2021. RAD51AP1 mediates RAD51 activity through nucleosome interaction. *J Biol Chem*: 100844.

Raderschall E, Stout K, Freier S, Suckow V, Schweiger S, Haaf T. 2002. Elevated levels of Rad51 recombination protein in tumor cells. *Cancer Res* **62**: 219-225.

Ray Chaudhuri A, Callen E, Ding X, Gogola E, Duarte AA, Lee JE, Wong N, Lafarga V, Calvo JA, Panzarino NJ et al. 2016. Replication fork stability confers chemoresistance in BRCA-deficient cells. *Nature* **535**: 382-387.

Recagni M, Bidzinska J, Zaffaroni N, Folini M. 2020. The Role of Alternative Lengthening of Telomeres Mechanism in Cancer: Translational and Therapeutic Implications. *Cancers (Basel)* **12**.

Rickman KA, Noonan RJ, Lach FP, Sridhar S, Wang AT, Abhyankar A, Huang A, Kelly M, Auerbach AD, Smogorzewska A. 2020. Distinct roles of BRCA2 in replication fork protection in response to hydroxyurea and DNA interstrand cross-links. *Genes & development* **34**: 832-846.

Ristic D, Wyman C, Paulusma C, Kanaar R. 2001. The architecture of the human Rad54-DNA complex provides evidence for protein translocation along DNA. *Proc Natl Acad Sci U S A* **98**: 8454-8460.

Roy U, Kwon Y, Marie L, Symington L, Sung P, Lisby M, Greene EC. 2021. The Rad51 paralog complex Rad55-Rad57 acts as a molecular chaperone during homologous recombination. *Molecular cell* **81**: 1043-1057 e1048.

Schlacher K, Christ N, Siaud N, Egashira A, Wu H, Jasin M. 2011. Double-strand break repair-independent role for BRCA2 in blocking stalled replication fork degradation by MRE11. *Cell* **145**: 529-542.

Sigurdsson S, Van Komen S, Petukhova G, Sung P. 2002. Homologous DNA pairing by human recombination factors Rad51 and Rad54. *J Biol Chem* **277**: 42790-42794.

Solinger JA, Heyer WD. 2001. Rad54 protein stimulates the postsynaptic phase of Rad51 protein-mediated DNA strand exchange. *Proc Natl Acad Sci U S A* **98**: 8447-8453.

Solinger JA, Lutz G, Sugiyama T, Kowalczykowski SC, Heyer WD. 2001. Rad54 protein stimulates heteroduplex DNA formation in the synaptic phase of DNA strand exchange via specific interactions with the presynaptic Rad51 nucleoprotein filament. *J Mol Biol* **307**: 1207-1221.

Song H, Xia SL, Liao C, Li YL, Wang YF, Li TP, Zhao MJ. 2004. Genes encoding Pir51, Beclin 1, RbAp48 and aldolase b are up or down-regulated in human primary hepatocellular carcinoma. *World J Gastroenterol* **10**: 509-513.

Spies J, Waizenegger A, Barton O, Surder M, Wright WD, Heyer WD, Lobrich M. 2016. Nek1 Regulates Rad54 to Orchestrate Homologous Recombination and Replication Fork Stability. *Molecular cell* **62**: 903-917.

Sung P. 1997a. Function of yeast Rad52 protein as a mediator between replication protein A and the Rad51 recombinase. *J Biol Chem* **272**: 28194-28197.

-. 1997b. Yeast Rad55 and Rad57 proteins form a heterodimer that functions with replication protein A to promote DNA strand exchange by Rad51 recombinase. *Genes & development* **11**: 1111-1121.

Sung P, Krejci L, Van Komen S, Sehorn MG. 2003. Rad51 recombinase and recombination mediators. *J Biol Chem* **278**: 42729-42732.

Swagemakers SM, Essers J, de Wit J, Hoeijmakers JH, Kanaar R. 1998. The human RAD54 recombinational DNA repair protein is a double-stranded DNA-dependent ATPase. *J Biol Chem* **273**: 28292-28297.

Symington LS. 2014. End resection at double-strand breaks: mechanism and regulation. *Cold Spring Harb Perspect Biol* **6**.

Taglialatela A, Alvarez S, Leuzzi G, Sannino V, Ranjha L, Huang JW, Madubata C, Anand R, Levy B, Rabadan R et al. 2017. Restoration of Replication Fork Stability in BRCA1- and BRCA2-Deficient Cells by Inactivation of SNF2-Family Fork Remodelers. *Molecular cell* **68**: 414-430 e418.

Tan TL, Essers J, Citterio E, Swagemakers SM, de Wit J, Benson FE, Hoeijmakers JH, Kanaar R. 1999. Mouse Rad54 affects DNA conformation and DNA-damage-induced Rad51 foci formation. *Curr Biol* **9**: 325-328.

Tanaka K, Hiramoto T, Fukuda T, Miyagawa K. 2000. A novel human rad54 homologue, Rad54B, associates with Rad51. *J Biol Chem* **275**: 26316-26321.

Tanaka K, Kagawa W, Kinebuchi T, Kurumizaka H, Miyagawa K. 2002. Human Rad54B is a double-stranded DNA-dependent ATPase and has biochemical properties different from its structural homolog in yeast, Tid1/Rdh54. *Nucleic Acids Res* **30**: 1346-1353.

Thakar T, Moldovan GL. 2021. The emerging determinants of replication fork stability. *Nucleic Acids Res*.

Thangavel S, Berti M, Levikova M, Pinto C, Gomathinayagam S, Vujanovic M, Zellweger R, Moore H, Lee EH, Hendrickson EA et al. 2015. DNA2 drives processing and restart of reversed replication forks in human cells. *J Cell Biol* **208**: 545-562.

Trenner A, Sartori AA. 2019. Harnessing DNA Double-Strand Break Repair for Cancer Treatment. *Front Oncol* **9**: 1388.

Van Komen S, Petukhova G, Sigurdsson S, Stratton S, Sung P. 2000. Superhelicity-driven homologous DNA pairing by yeast recombination factors Rad51 and Rad54. *Molecular cell* **6**: 563-572.

Wesoly J, Agarwal S, Sigurdsson S, Bussen W, Van Komen S, Qin J, van Steeg H, van Benthem J, Wassenaar E, Baarends WM et al. 2006. Differential contributions of mammalian Rad54 paralogs to recombination, DNA damage repair, and meiosis. *Mol Cell Biol* **26**: 976-989.

Wiese C, Dray E, Groesser T, San Filippo J, Shi I, Collins DW, Tsai MS, Williams GJ, Rydberg B, Sung P et al. 2007. Promotion of homologous recombination and genomic stability by RAD51AP1 via RAD51 recombinase enhancement. *Molecular cell* **28**: 482-490.

Wiese C, Hinz JM, Tebbs RS, Nham PB, Urbin SS, Collins DW, Thompson LH, Schild D. 2006. Disparate requirements for the Walker A and B ATPase motifs of human RAD51D in homologous recombination. *Nucleic Acids Res* **34**: 2833-2843.

Xia B, Sheng Q, Nakanishi K, Ohashi A, Wu J, Christ N, Liu X, Jasin M, Couch FJ, Livingston DM. 2006. Control of BRCA2 cellular and clinical functions by a nuclear partner, PALB2. *Molecular cell* **22**: 719-729.

Xu ZY, Loignon M, Han FY, Panasci L, Aloyz R. 2005. Xrcc3 induces cisplatin resistance by stimulation of Rad51-related recombinational repair, S-phase checkpoint activation, and reduced apoptosis. *J Pharmacol Exp Ther* **314**: 495-505.

Zafar F, Seidler SB, Kronenberg A, Schild D, Wiese C. 2010. Homologous recombination contributes to the repair of DNA double-strand breaks induced by high-energy iron ions. *Radiat Res* **173**: 27-39.

Zellweger R, Dalcher D, Mutreja K, Berti M, Schmid JA, Herrador R, Vindigni A, Lopes M. 2015. Rad51-mediated replication fork reversal is a global response to genotoxic treatments in human cells. *J Cell Biol* **208**: 563-579.

Zhang Z, Fan HY, Goldman JA, Kingston RE. 2007. Homology-driven chromatin remodeling by human RAD54. *Nat Struct Mol Biol* **14**: 397-405.

Zhao H, Gao Y, Chen Q, Li J, Ren M, Zhao X, Yue W. 2020. RAD51AP1 promotes progression of ovarian cancer via TGF-beta/Smad signalling pathway. *J Cell Mol Med*.

Zhao W, Steinfeld JB, Liang F, Chen X, Maranon DG, Jian Ma C, Kwon Y, Rao T, Wang W, Sheng C et al. 2017. BRCA1-BARD1 promotes RAD51-mediated homologous DNA pairing. *Nature* **550**: 360-365.

Zhao W, Vaithiyalingam S, San Filippo J, Maranon DG, Jimenez-Sainz J, Fontenay GV, Kwon Y, Leung SG, Lu L, Jensen RB et al. 2015. Promotion of BRCA2-

Dependent Homologous Recombination by DSS1 via RPA Targeting and DNA Mimicry. *Molecular cell* **59**: 176-187.

Zhuang L, Zhang Y, Meng Z, Yang Z. 2020. Oncogenic Roles of RAD51AP1 in Tumor Tissues Related to Overall Survival and Disease-Free Survival in Hepatocellular Carcinoma. *Cancer Control* **27**: 1073274820977149.

Figures

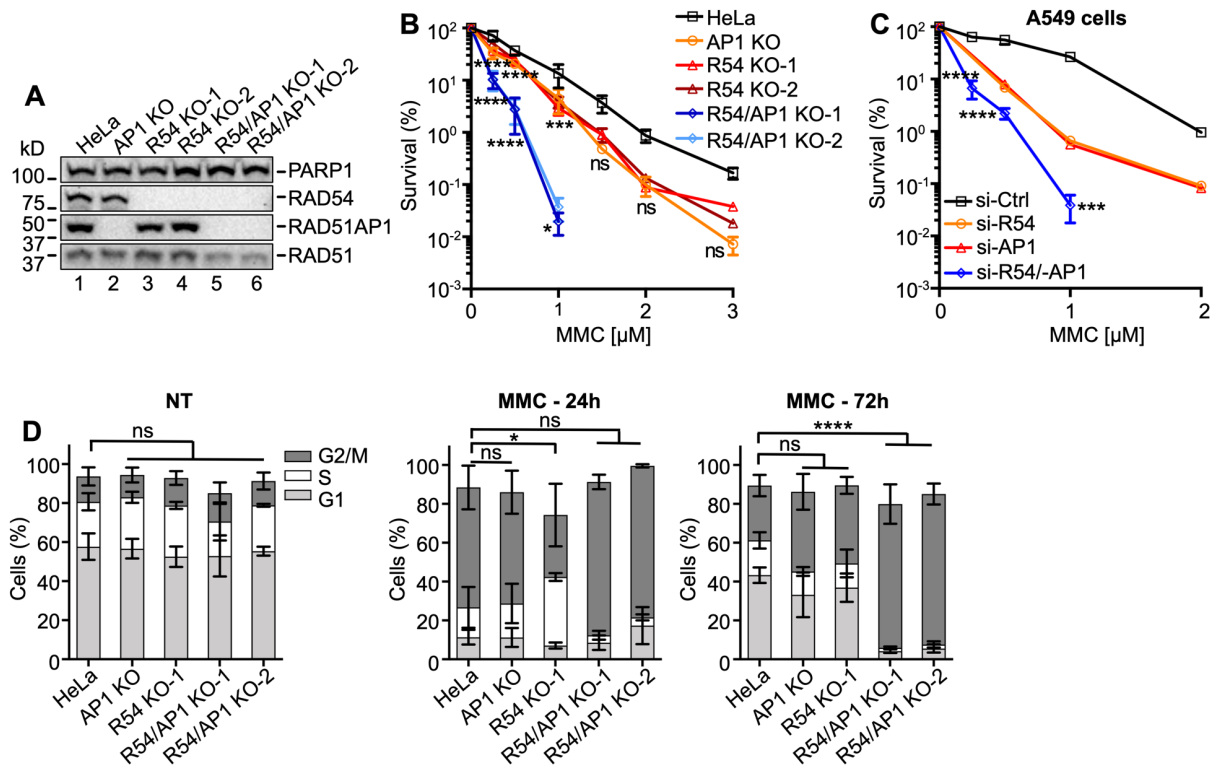

Figure 1. Deficiency of both *RAD51AP1* and *RAD54* synergistically affects MMC cytotoxicity and cell cycle progression. (*A*) Western blots of nuclear extracts of HeLa cells and derivatives. *RAD51AP1* KO cells (here: AP1 KO), two independently isolated *RAD54* KO cell lines (here: R54 KO-1, R54 KO-2), and two independently isolated *RAD54*/*RAD51AP1* KO cell lines (here: R54/AP1 KO-1; R54/AP1 KO-2). The signal for PARP1 serves as loading control. (*B*) Results from clonogenic cell survival assays after MMC. Data points are the means from 2-5 independent experiments ±SD. ***, $p < 0.001$; ****, $p < 0.0001$; ns, non-significant; two-way ANOVA test followed by Dunnett's multiple comparisons test. (*C*) Results from clonogenic cell survival assays of MMC-treated A549 cells with RAD51AP1 and/or RAD54 knockdown. Data points are the means from three technical replicates for A549 cells transfected with RAD54 siRNA (here: si-R54) or RAD51AP1 siRNA (si-AP1), and from two independent experiments ±SD for A549 cells transfected with negative control siRNA (si-Ctrl) or RAD54 and RAD51AP1 siRNA (si-R54/-AP1). ***, $p < 0.001$; ****, $p < 0.0001$; two-way ANOVA test followed by Sidak's

multiple comparisons test. (*D*) Average percentage of cells in G1, S and G2/M cell cycle phases without (here: NT (no treatment)), and 24 and 72 h after release from MMC. Bars are the means from at least three independent experiments ±SD. *, $p < 0.05$, ****, $p < 0.0001$, ns, non-significant; one-way ANOVA test followed by Dunnett's multiple comparisons test.

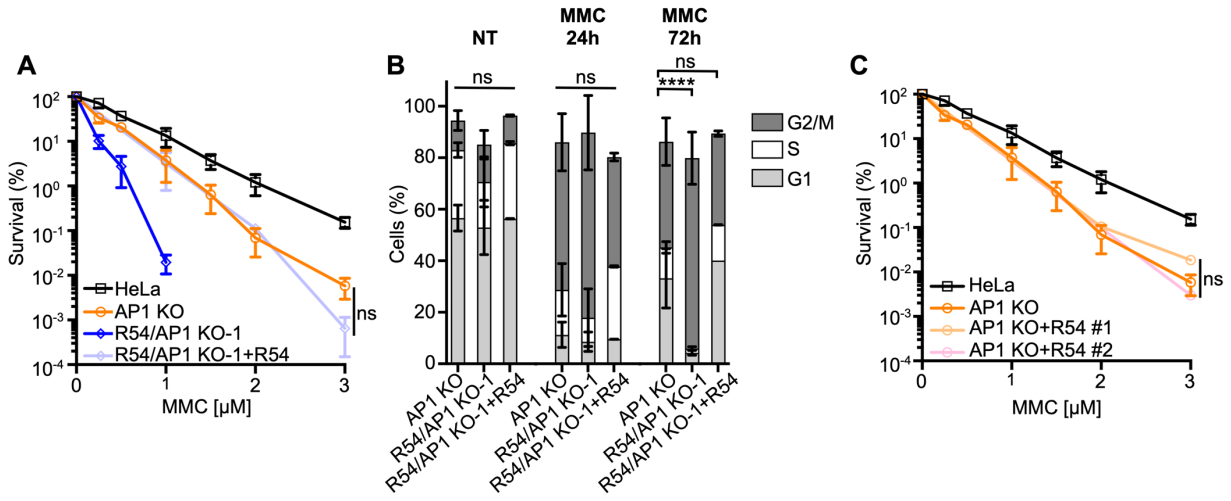

Figure 2. Ectopic expression of RAD54 rescues *RAD54* deficiency in *RAD54*/*RAD51AP1* double KO cells. (*A*) Results from MMC clonogenic cell survival assays of *RAD54*/*RAD51AP1* double KO cells (R54/AP1 KO-1) with (here: +R54) and without ectopic RAD54 and of *RAD51AP1* KO (AP1 KO) and HeLa cells for comparison purposes. Data points are the means from two independent experiments ±SD. ns: non-significant; two-way ANOVA test followed by Tukey's multiple comparisons test. (*B*) Average percentage *RAD54*/*RAD51AP1* double KO cells with (here: +R54) and without ectopic RAD54 and of *RAD51AP1* KO cells in G1, S and G2/M cell cycle phases without MMC (NT), and 24 h and 72 h after release from MMC. Bars represent the means from two independent experiments ±SD. ****, $p < 0.0001$; ns, non-significant; one-way ANOVA test followed by Dunnett's multiple comparisons test. (*C*) Results from MMC clonogenic cell survival assays of *RAD51AP1* KO cells and two independently isolated *RAD51AP1* KO clones expressing different amounts of ectopic RAD54-HA (see Supplemental Fig. S2A). Data points are the means from two independent experiments ±SD for AP1 KO+R54 #1

cells and from three technical replicates for AP1 KO+R54 #2 cells. ns, non-significant; two-way ANOVA test followed by Tukey's multiple comparisons test.

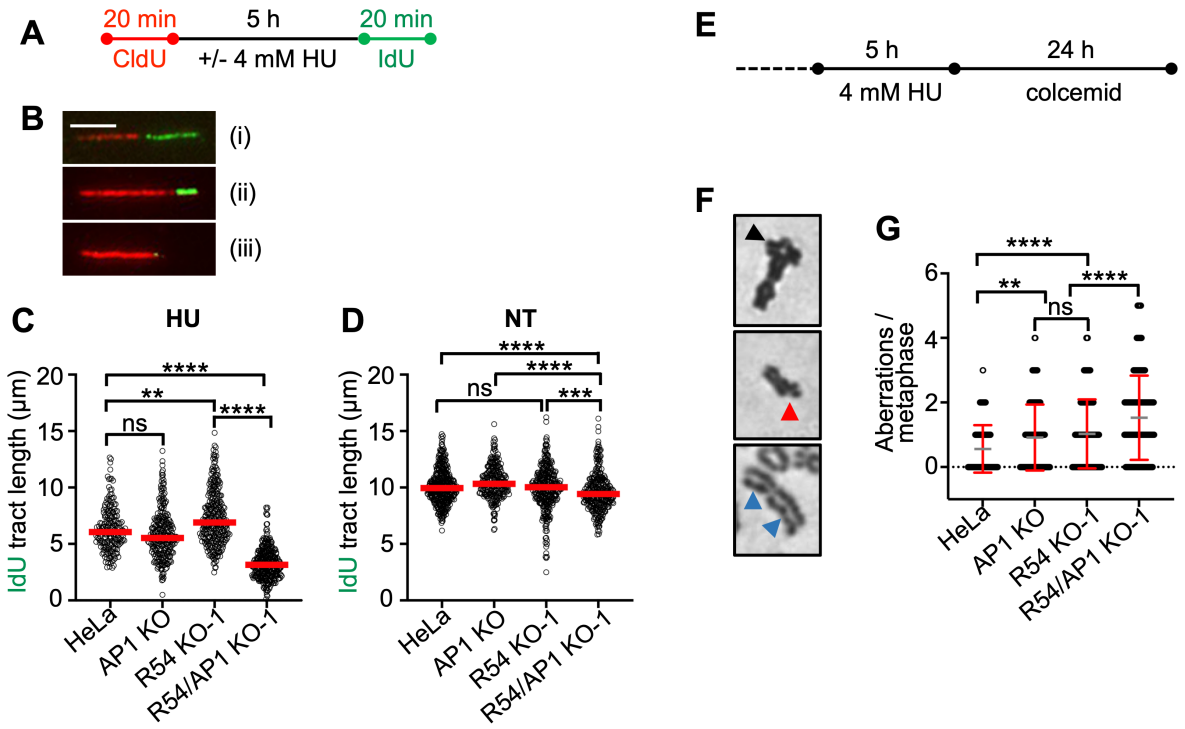

Figure 3. Concomitant loss of *RAD51AP1* and *RAD54* results in increased replication stress and genome instability. (*A*) Schematic of the experimental protocol for the DNA fiber assay. (*B*) Representative micrographs of fiber tracts of a restarted (i), a delayed (ii), and a replication fork that failed to restart (iii). Scale bar: 10 µm. (*C*) Median IdU tract length (green) after HU of *RAD51AP1* KO (AP1 KO), *RAD54* KO (R54 KO-1), and *RAD54*/*RAD51AP1* double KO (R54/AP1 KO-1) cells. Data points are from 100-150 fibers of two independent experiments each, with medians (red lines). **, $p < 0.01$; ****, $p < 0.0001$; ns, non-significant; Kruskal-Wallis test followed by Dunn's multiple comparisons test. (*D*) Median IdU tract length (green) under unperturbed conditions (NT). Data points are from 100-150 fibers of two independent experiments each, with medians (red lines). **, $p < 0.01$; ***, $p < 0.001$; ****, $p < 0.0001$; ns, non-significant; Kruskal-Wallis test followed by Dunn's multiple comparisons test. (*E*) Schematic of the experimental protocol to induce chromosomal aberrations. (*F*) Representative micrographs of chromosomal

aberrations after HU; radial (black arrow), chromatid break (red arrow) and chromatid gaps (blue arrows). (*G*) Aberrations per metaphase after HU in *RAD51AP1* KO (AP1 KO), *RAD54* KO (R54 KO-1), and *RAD54*/*RAD51AP1* double KO (R54/AP1 KO-1) cells. Data points are from 100 metaphases of two independent experiments each. Means (grey) ±SD (red) are shown. **, $p < 0.01$; ****, $p < 0.0001$; ns, non-significant; one-way ANOVA test followed by Tukey's multiple comparisons test.

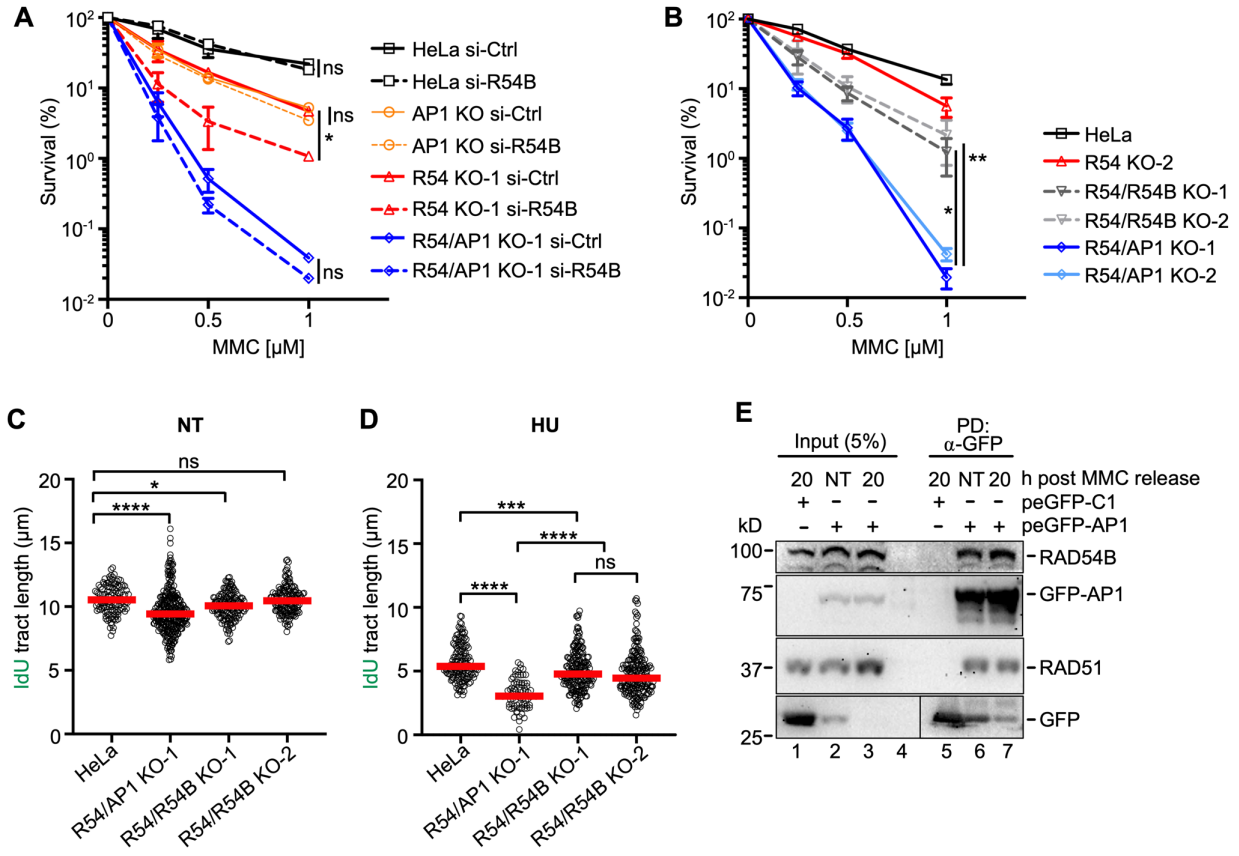

Figure 4. Concomitant loss of *RAD54* and *RAD54B* exacerbates MMC cytotoxicity and replication stress less extensively than concomitant loss of *RAD54* and *RAD51AP1*. (*A*) Results from clonogenic cell survival assays after MMC of cells transfected with negative control (si-Ctrl) or RAD54B siRNA (si-R54B); HeLa, *RAD51AP1* KO (AP1 KO), *RAD54* KO (R54 KO-1), *RAD54*/*RAD51AP1* double KO (R54/AP1 KO-1) cells. Data points are the means from two independent experiments ±SD. *, $p < 0.05$; ns, non-significant; two-way ANOVA test followed by Tukey's multiple comparisons test. (*B*) Results from

clonogenic cell survival assays after MMC treatment of HeLa, *RAD54* KO (R54 KO-2), *RAD54*/*RAD54B* double KO (R54/54B KO-1, KO-2), and *RAD54*/*RAD51AP1* double KO (R54/AP1 KO-1, KO-2) cells. Data points are the means from two independent experiments ±SD. *, $p < 0.05$; **, $p < 0.01$; two-way ANOVA test followed by Dunnett's multiple comparisons test. (*C*) Median IdU tract length under unperturbed conditions (NT) of HeLa, *RAD54*/*RAD51AP1* double KO (R54/AP1 KO-1), and *RAD54*/*RAD54B* double KO (R54/54B KO-1, KO-2) cells. Data points are from 150-300 fibers of one experiment, with medians (red lines). *, $p < 0.05$; ****, $p < 0.0001$; ns, non-significant; Kruskal-Wallis test followed by Dunn's multiple comparisons test. (*D*) Median IdU tract lengths after HU of HeLa, *RAD54*/*RAD51AP1* double KO (R54/AP1 KO-1), and *RAD54*/*RAD54B* double KO (R54/54B KO-1, KO-2) cells. Data points are from 150-200 fibers of one experiment, with medians (red lines). ***, $p < 0.001$; ****, $p < 0.0001$; ns, non-significant; Kruskal-Wallis test followed by Dunn's multiple comparisons test. (*E*) Western blots to show that endogenous RAD54B co-precipitates in anti-eGFP protein complexes from *RAD54*/*RAD51AP1* KO cells ectopically expressing eGFP-RAD51AP1 (here: peGFP-AP1) in the absence of MMC (NT; lane 6) and 20 h after a 2-h incubation in 0.5 μM MMC (lane 7). RAD51: positive control for interaction, as previously shown in different cell types (Kovalenko et al. 1997; Wiese et al. 2007). Lane 5: Neither RAD54B nor RAD51 co-precipitate in anti-eGFP protein complexes generated from *RAD54*/*RAD51AP1* KO cells transfected with control plasmid (peGFP-C1).

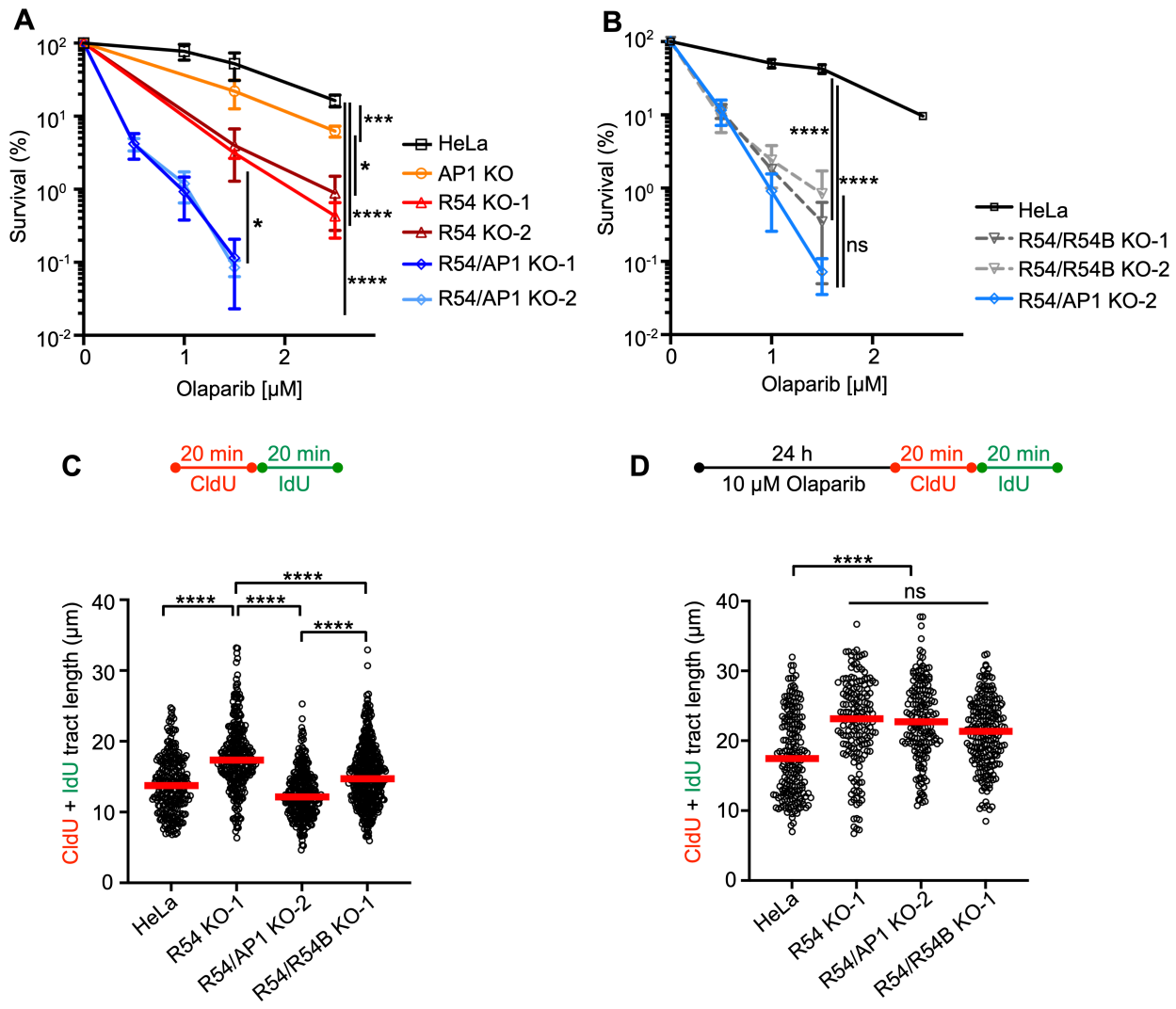

Figure 5. Loss of *RAD54* and *RAD51AP1* or of *RAD54* and *RAD54B* synergistically enhances cellular sensitivity to olaparib. (A) Results from clonogenic cell survival assays in the presence of olaparib of HeLa, *RAD51AP1* KO (AP1 KO), *RAD54* KO (R54 KO-1, KO-2), and *RAD54*/*RAD51AP1* double KO (R54/AP1 KO-1, KO-2) cells. Data points are the means from two independent experiments ±SD. *, $p < 0.05$; ***, $p < 0.001$; ****, $p < 0.0001$; ns, non-significant; two-way ANOVA test followed by Tukey's multiple comparisons test. (B) Results from clonogenic cell survival assays in the presence of olaparib of HeLa, *RAD54*/*RAD54B* double KO (R54/R54B KO-1, KO-2), and *RAD54*/*RAD51AP1* double KO (R54/AP1 KO-2) cells. Data points are the means from two independent experiments ±SD. ****, $p < 0.0001$; ns, non-significant; two-way ANOVA test followed by Tukey's multiple comparisons test. (C) Schematic of the experimental

protocol for the DNA fiber assay in unperturbed cells. Total tract length (CldU+IdU) of DNA fibers from HeLa, *RAD54* KO (R54 KO-1), *RAD54*/*RAD51AP1* double KO (R54/AP1 KO-2), and *RAD54*/*RAD54B* double KO (R54/R54B KO-1) cells. Data points are from 100-150 fibers of two independent experiments each, with medians (red lines). ****, $p < 0.0001$; Kruskal-Wallis test followed by Dunn's multiple comparisons test. (E) Schematic of the experimental protocol for the DNA fiber assay after olaparib. Total tract length (CldU+IdU) of DNA fibers from HeLa, *RAD54* KO (R54 KO-1), *RAD54*/*RAD51AP1* double KO (R54/AP1 KO-2), and *RAD54*/*RAD54B* double KO (R54/R54B KO-1) cells. Data points are from 150-200 fibers of one experiment, with medians (red lines). ****, $p < 0.0001$; ns, non-significant; Kruskal-Wallis test followed by Dunn's multiple comparisons test.

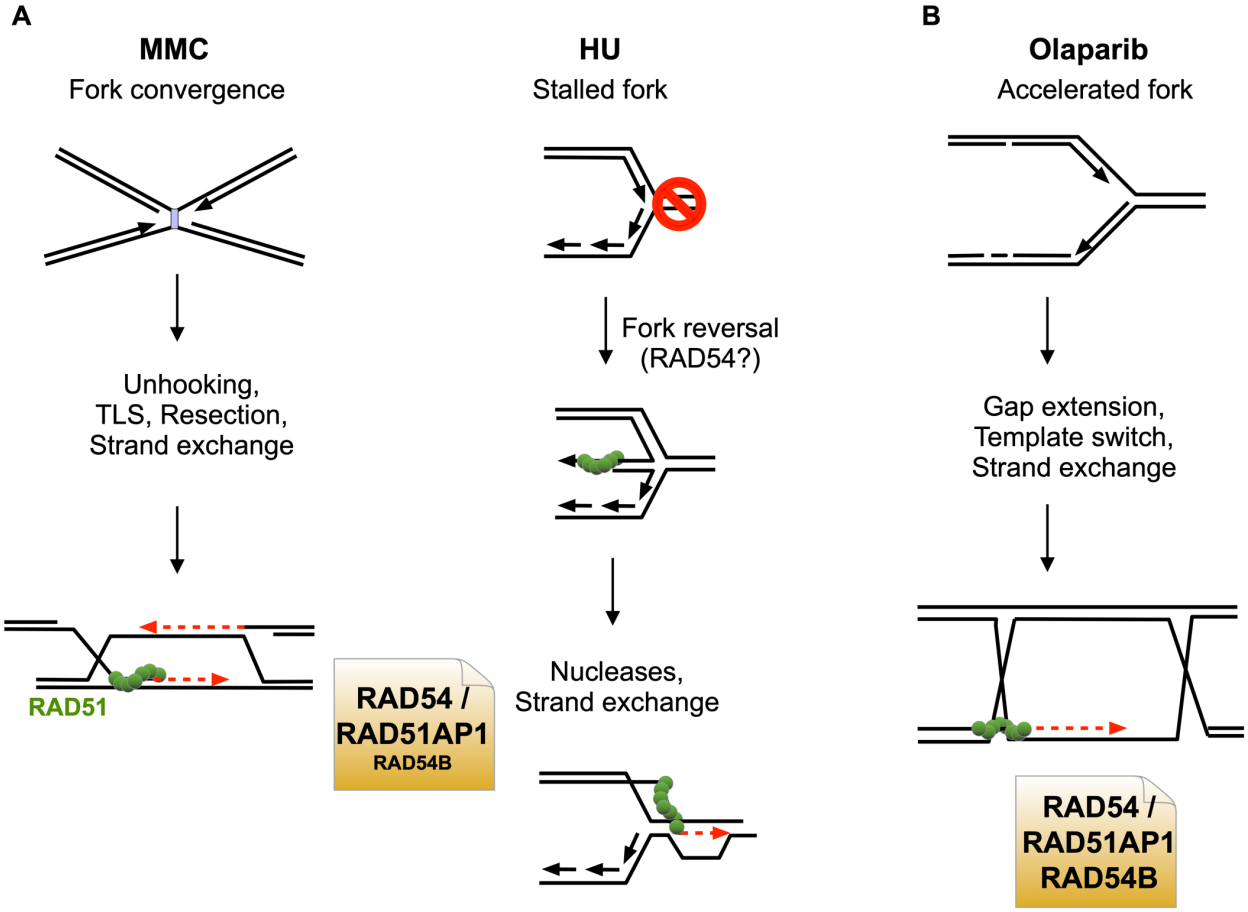

Figure 6. Model depicting the synthetic interaction between RAD54 and RAD51AP1 (A, B) and between RAD54 and RAD54B (B). For details see text.